Appl Phys A (2009) 94: 111–115
DOI 10.1007/s00339-008-4925-0

Applied Physics A
Materials Science & Processing

Melt-mediated coalescence of solution-deposited ZnO nanoparticles by excimer laser annealing for thin-film transistor fabrication

Heng Pan · Nipun Misra · Seung H. Ko · Costas P. Grigoropoulos · Nate Miller · Eugene E. Haller · Oscar Dubon

Received: 10 September 2008 / Accepted: 29 September 2008 / Published online: 19 October 2008

Abstract Nanoparticle solutions are considered promising for realizing low cost printable high performance flexible electronics. In this letter, excimer laser annealing (ELA) was employed to induce melting of solution-deposited ZnO nanoparticles and form electrically conductive porous films. The properties of the films were characterized by scanning electron microscopy, high-resolution transmission electron microscopy, DC conductance, and photoluminescence measurements. Thin-film field-effect transistors have been fabricated by ELA without the use of conventional vacuum or any high temperature thermal annealing processes. The transistors show n-type accumulation mode behavior with mobility greater than 0.1 cm^2/V s and current on/off ratios of more than 10^4. Optimization and control of the laser processing parameters minimized thermal impact on the substrate. This technique can be beneficial in the fabrication of metal oxide based electronics on heat sensitive flexible plastic substrates using low-cost, large-area solution processing combined with direct printing techniques.

PACS 81.07.Wx · 81.15.-z · 81.15.Fg · 81.16.-c · 81.16.Mk

H. Pan · N. Misra · S.H. Ko (✉) · C.P. Grigoropoulos
Laser Thermal Laboratory, Department of Mechanical Engineering, University of California, Berkeley, CA 94720-1740, USA
e-mail: max93ko@gmail.com

C.P. Grigoropoulos (✉)
e-mail: cgrigoro@me.berkeley.edu

N. Miller · E.E. Haller · O. Dubon
Department of Materials Science & Engineering, University of California, Berkeley, CA, USA

N. Miller · E.E. Haller · O. Dubon
Materials Sciences Division, Lawrence Berkeley National Laboratory, Berkeley, CA 94720, USA

1 Introduction

Due to its wide band gap and large piezoelectric constant, zinc oxide (ZnO) has drawn attention for its potential applications in a broad range of fields such as room-temperature UV lasing [1], transparent conducting electrodes [2], gas sensors [3], solar cells [4], and surface-acoustic-wave devices [5]. There have been a number of recent reports on field-effect transistors (FETs) using ZnO as the active channel layer [6–8]. These transistors have high visual transparency and electrical mobility and are stable in air. ZnO deposition at room temperature over large areas was reported [6, 9, 10] with mobility between 0.01 and 25 cm^2/V s and an on/off ratio from 10^3 to 10^7. This suggests compatibility with flexible polymer substrates. However, most such ZnO films have been formed by vacuum deposition methods: sputtering, RF sputtering, or pulsed-laser deposition [6–8]. As an alternative cost-effective ZnO deposition method, solution-deposited ZnO FETs have been demonstrated recently without using vacuum processes [11–13]. However, the reported solution-deposition methods need high temperature annealing processes that are not compatible with flexible polymer substrates. Chemical solution methods, such as sol–gel [11], require annealing steps above 600°C. Simple solution processing of ZnO nanoparticles (NPs) reported to date such as spin coating, dip coating, or ink-jet printing [12, 13] also involve a high temperature post-deposition thermal annealing/sintering step (>300°C), making these processes incompatible with plastic substrates. The use of a pulsed laser is therefore more advantageous for the annealing because laser heating is highly local and very rapid. Excimer laser annealing (ELA) has previously been used in place of thermal annealing of thin films [14] and nanowires [15] to provide compatibility with heat-sensitive materials. In this letter, we demonstrate solution-deposited

and excimer laser annealed ZnO NPs as an active channel layer to obtain ZnO NP FETs without using any vacuum or high temperature thermal annealing processes.

2 Experimental method

The ZnO NP solution was prepared by dispersing ZnO nanopowders (<100 nm, Sigma Aldrich) in ethanol (3.5% wt.). The ZnO NP dispersion was sonicated for 1 h before use. A drop (0.7 μL) of ZnO dispersion was applied to the substrate, and capillary spreading formed a uniform ZnO NP film. The ZnO NP film can also be obtained by spin coating. For spin coating, ethylene glycol (EG) should be added (EG vs. ethanol = 1:10) to adjust the evaporation rate in order to obtain uniform NP films. A krypton fluoride (KrF) excimer laser (wavelength: 248 nm, pulse width (full width at half maximum: 20 ns)) was used to anneal the ZnO NPs. A large-area, uniform, top-flat beam profile of 11 × 11 mm^2 was obtained by using a fly's eye homogenizer to ensure uniform laser annealing. Scanning electron microscopy (SEM) and high resolution transmission electron microscopy (HRTEM) were employed to examine the structural changes. A DC conductance measurement was performed to characterize the electrical properties. To examine the optical properties, photoluminescence (PL) measurements were performed. The PL system uses a SPEX 1404 0.85-m double spectrometer and a room-temperature photomultiplier tube detector. The excitation source is the 325-nm line of a HeCd laser. Measurements were performed at room temperature in the backscattering geometry. To fabricate thin-film transistors, ZnO NP solution was applied on pre-patterned metal contacts followed by laser annealing. Figure 1 shows a schematic of the laser annealing process and a thin-film FET structure. The ZnO thin-film FETs have a typical bottom gate/bottom contact transistor configuration with a highly doped n-type silicon wafer as the back gate and a 100-nm-thick SiO_2 layer as the gate dielectric. Gold source and drain electrodes were defined by a standard lift-off technique. The channel length (L) was varied from 2 to 20 μm and the channel width (W) was fixed at 160 μm. The absorption efficiency can be calculated from the ZnO complex refractive index ($\mathbf{n} = 1.8 + 0.43i$ at 248 nm) [16] for bulk material. The absorption efficiency of two ZnO nanoparticles (80-nm diameter) was calculated by the discrete dipole approximation to be in the range of 0.95–1.2 depending on interparticle spacing. This signifies that the particle density needs to be optimized in order to maximize laser energy coupling.

3 Results and discussion

Excimer laser annealing induces structural, electrical, and optical property changes in ZnO NP films. Figure 2a shows the SEM images of single laser pulse annealed microstructures at three different laser fluences (100, 130, and 160 mJ/cm^2 from left to right). At low laser fluences (≤130 mJ/cm^2), pulsed-laser annealing kept intact the structural properties of nanostructured films. At the fluence of 160 mJ/cm^2, large interconnected grains surrounded by voids were formed after annealing. It has been reported that excimer laser fluences larger than 130 mJ/cm^2 can induce melting of ZnO nanoparticles [17]. The fact that laser heating of NP films up to melting strongly changes microstructures is confirmed from the observations by TEM. Figure 2b shows the TEM image of NP films after annealing with 160 mJ/cm^2. The discretely facetted nanocrystals were transformed into rounded and smooth agglomerations after annealing. Moreover, the grain boundaries of the crystallites

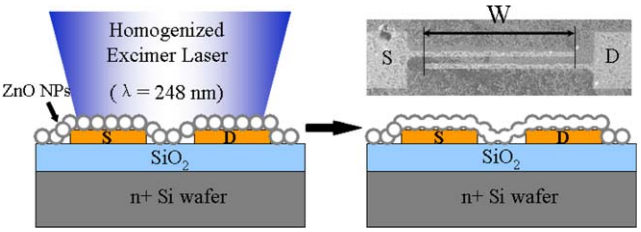

Fig. 1 Schematic side view of the excimer laser annealing process and the ZnO NP FET structure. 'S' and 'D' indicate source and drain electrodes, respectively. *Right top inset* is the top-view SEM image of transistor electrodes with a layer of deposited ZnO NPs. *Inset arrow* corresponds to 160 μm

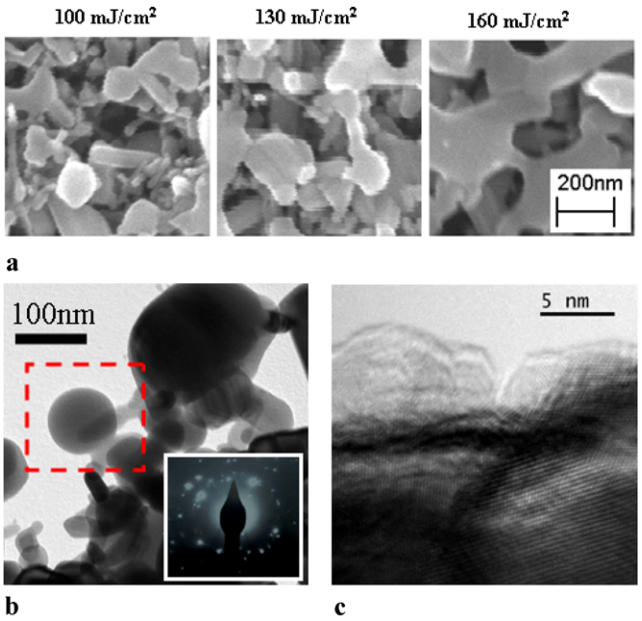

Fig. 2 (**a**) SEM pictures of nanostructure changes of ZnO NP film after irradiation with different excimer laser fluences. (**b**) TEM image of ZnO NP film after excimer laser irradiation. *Inset* shows the diffraction pattern from the marked region. (**c**) The HRTEM image reveals the polycrystalline structure of the laser-processed ZnO NP film

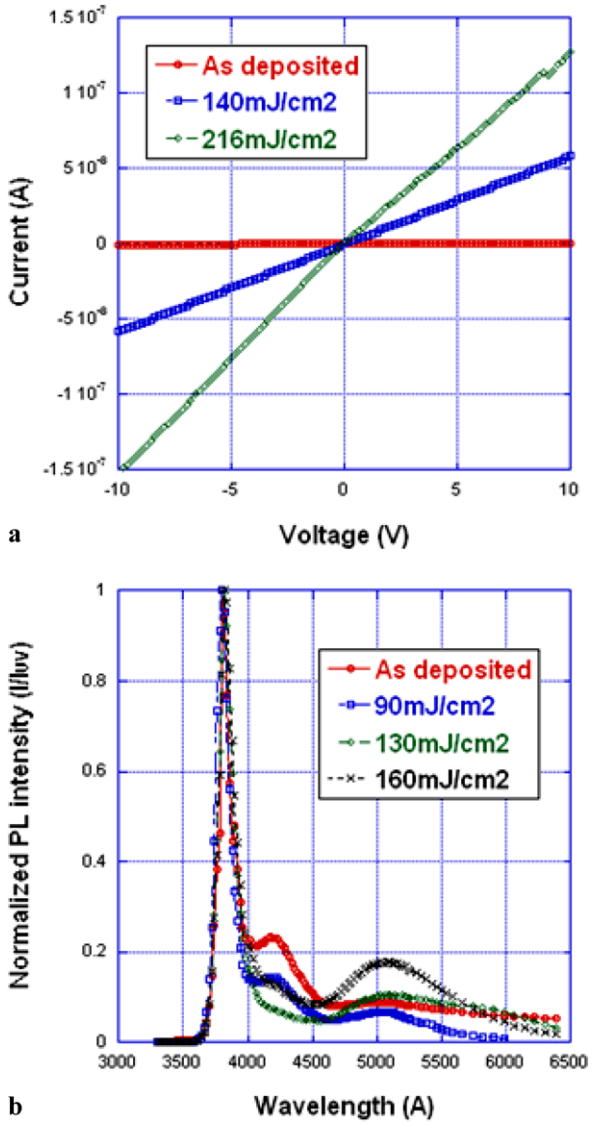

Fig. 3 (**a**) Room-temperature I–V data for an Al ohmic contact to ZnO NP film after laser processing at different fluences. (**b**) Room-temperature PL spectra with and without laser annealing

within agglomerations can be clearly seen in the HRTEM image (Fig. 2c). The polycrystalline structure, further confirmed by the electron diffraction pattern from the marked region, should be expected after ns laser induced melting and subsequent resolidification. Based on our previous in situ measurement of the resolidification/cooling time for supported NPs (∼tens of ns) [18] and reported measurements for suspended NPs (5 ns to 1 μs) [19], the quenching rate can be estimated to be lower than 10^{11} K/s, insufficient to obtain amorphous structures. For DC conductance measurement, Al ohmic contacts were made to both as-deposited NP and laser-annealed porous films. Figure 3a shows the room-temperature dark I–V characteristics of the Al contacts at different laser fluences. Measurements showed that the resistance between 1.4 cm spaced contacts was determined to be 3.4×10^4 MΩ for a film without laser annealing, 171 MΩ for one annealed at 140 mJ/cm^2, and 78 MΩ for one annealed at 216 mJ/cm^2. The resistance was reduced by three orders of magnitude by laser annealing and linear I–V behavior was exhibited in all samples. Figure 3b shows the room-temperature normalized PL (I/I_{UV}) spectra of ZnO samples as a function of wavelength for solution-deposited films with and without laser annealing. Three major emission bands can be seen: UV near-band-edge emission (381 nm) and defect-related violet (420 nm) and green (500 nm) emissions. At a laser fluence of 90 mJ/cm^2, below the melting threshold, it is found that UV emission increases as exhibited by a reduction of both defect-related emissions in the normalized PL (Fig. 3b). Further increasing of laser fluence reduces the violet emission until a substantial level of melting is seen at a laser fluence of 160 mJ/cm^2. On the other hand, the green emission band located at 500 nm, commonly attributed to oxygen vacancies [20], is found to increase with laser annealing. This is due to the fact that the high photon energy of the excimer laser can break chemical bonds, create oxygen vacancies, and remove excess oxygen [21].

The inset in Fig. 4a shows a SEM image of the ZnO NP FET channel with laser annealing. The SEM image reveals no observable damage to substrate and electrodes after laser annealing. The particles are distributed homogeneously with a high degree of porosity that is consistent with a high surface area structure between electrodes. The electrical characteristics of individual transistors were measured using an Agilent 4155A semiconductor analyzer in a dark Faraday cage. Figure 4a shows the output characteristics of a laser-annealed ZnO FET with a W/L of 160/12 μm. The source–drain voltage (V_{DS}) was scanned from 0 to 2 V while the gate voltage (V_{GS}) was fixed at −15 V (circles), 0 V (crosses), 15 V (squares), and 30 V (triangles). The shown maximum V_{DS} has been limited to 2 V because a strong shift of V_{T} to negative values and punch-through could be observed when a higher V_{DS} was used. This is due to the fact that the annealed film is relatively thick and the laser processing is limited to the film's surface region; then, the region close to the gate is less laser processed and gate modulation is less efficient. Using smaller NPs and forming an optically and physically thinner film can remedy this issue. Therefore, device operation is shown only in the linear region here. Figure 4b shows the corresponding transfer characteristics. The gate voltage was scanned from −30 to +30 V while the drain voltage was fixed at 1 V (triangles) and 2 V (squares). The transfer characteristic graph indicates that the transistor operates in an n-channel accumulation mode. A semilog plot of I_{D} vs. V_{G} (not shown here) also shows an on/off current ratio of $>10^4$ with a very low off-current level (∼10 pA), a sub-threshold slope of 5 V/decade, and a threshold voltage (V_{T}) of 5 V. The transconductance

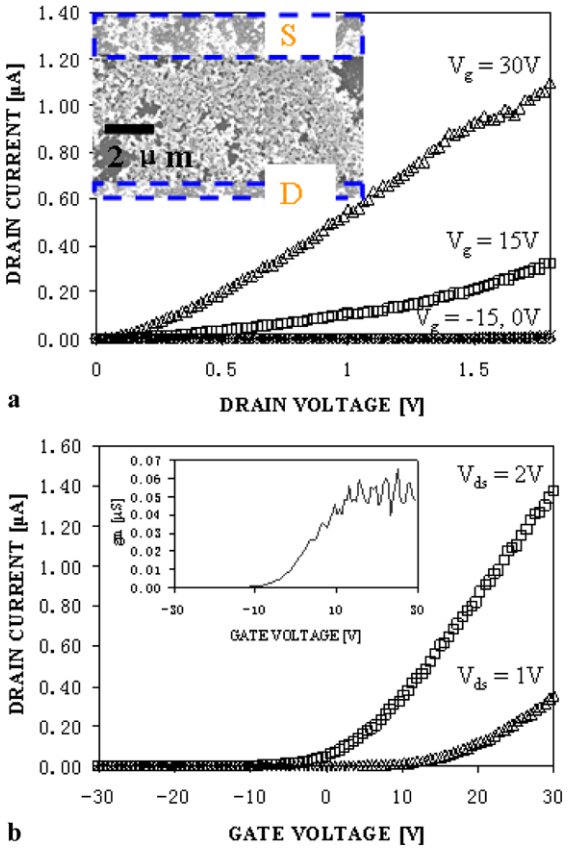

Fig. 4 (**a**) Output characteristics of an excimer laser annealed ZnO NP FET with $W/L = 160/12$ μm. *Inset* shows SEM image of the channel region covered by laser-annealed NPs. Drain voltage was scanned from 0 to 2 V while gate voltage was fixed at −15 V (*circles*), 0 V (*crosses*), 15 V (*squares*), and 30 V (*triangles*). (**b**) Transfer characteristics of the device. The gate voltage was scanned from −30 to +30 V while the drain voltage was fixed at 1 V (*triangles*) and 2 V (*squares*). *Inset graph* is a transconductance curve of the device when the drain voltage was 2 V. The saturation value is 50 nS

(g_m) is 50 nS as shown in Fig. 4b inset graph. The effective field effect mobility (μ) of the ZnO nanoparticle porous film FET can be derived using the following relationship for the continuous thin film:

$$\mu = \frac{L g_m}{W C_{ox} V_{DS}}, \quad (1)$$

where L, W, and C_{ox} indicate the channel length, channel width, and capacitance, respectively. We point out that due to the geometry of the porous film and the absence of a simple estimate of capacitance, we have used an effective mobility assuming complete coverage. The effective mobility estimated in this manner is a lower-bound value. The effective field effect mobility extracted using this equation and the measured dimensions is estimated to be 0.106 cm^2/V s. The laser-annealed ZnO FETs show three to four orders of magnitude higher mobility and on/off ratio compared with unannealed devices. In addition, a reliable electrical contact can be expected following direct annealing of the semiconductor material on the electrodes. It should be noted that the mobility of the laser-annealed ZnO measured here is comparable to the highest value (0.1–0.2 cm^2/V s) reported for solution-deposited and thermally annealed (at a temperature of ∼700°C) ZnO NP n-type FETs [12]. Laser annealing of ZnO NPs enabled a reasonably good mobility without high temperature thermal annealing of the selected area. However, this value is still lower than the published ZnO thin film mobility (∼10 cm^2/V s) for sputtered or pulsed-laser-deposited ZnO thin-film transistors [8]. Possible reasons for this could be due to porous structure, less actual coverage ratio, increased carrier scattering by significant film porosity, large surface area, and large impurity concentrations in the film. Also, note that the gate leakage current reported here is very low (∼10 nA) compared to the previously reported high gate leakage current, since ZnO attacks the insulating SiO_2 layer during the high-temperature annealing (>600°C) [11]. The low gate leakage obtained in this work signifies that ELA minimized thermal effects on the SiO_2/n + Si substrate while providing sufficient energy to induce particle annealing and coalescence.

4 Conclusions

In conclusion, excimer laser annealing of solution-deposited ZnO NPs for high-performance n-type FET fabrication was demonstrated without using any vacuum process or high temperature thermal annealing process. A single laser pulse of 160-mJ/cm^2 fluence could transform solution-deposited discrete ZnO NPs into interconnected porous structures, thus enhancing the electrical mobility. The remarkable improvement of the FET performance with low gate leakage current and intact underlying electrodes after laser annealing signifies that the current process can be used potentially for low-temperature, low-cost flexible electronics on heat sensitive polymer substrates. This process can be easily integrated with recently developed metal NP ink-jet printing and selective laser sintering [22–24] or metal NP direct nanoimprinting [25] for low-temperature, high-resolution FET electrode fabrication. Current solution-deposited and laser-annealed ZnO NP FETs can replace low-mobility semiconducting polymer to achieve cost-effective, all-printing, low-temperature, lithography-free, and high-performance electronics on polymer substrates.

Acknowledgements Financial support to the University of California, Berkeley by the US National Science Foundation under Grant No. CMMI 0700827 is gratefully acknowledged. The authors also would like to thank Xiaobo Chen from Lawrence Berkeley National Laboratory for HRTEM characterizations and discussions. PL measurements were supported by the Director, Office of Science, Office of Basic Energy Sciences, Division of Materials Sciences and Engineering, of the US Department of Energy under Contract No. DE-AC02-05CH11231.

References

1. X.W. Sun, S.F. Yu, C.X. Xu, C. Yuen, B.J. Chen, S. Li, Jpn. J. Appl. Phys. Part 2 **42**, L1229 (2003)
2. T. Minami, Semicond. Sci. Technol. **20**, S35 (2005)
3. G.Q. Ding, M.J. Zheng, W.L. Xu, W.Z. Shen, Nanotechnology **16**, 1285 (2005)
4. M. Law, L.E. Greene, J.C. Johnson, R. Saykally, P. Yang, Nature Mater. **4**, 455 (2005)
5. J.J. Chen, F. Zeng, D.M. Li, J.B. Niu, F. Pan, Thin Solid Films **485**, 257 (2005)
6. R.F. Carcia, R.S. McLean, M.H. Reilly, G. Nunes Jr., Appl. Phys. Lett. **82**, 1117 (2003)
7. R.L. Hoffman, B.J. Norris, J.F. Wager, Appl. Phys. Lett. **82**, 733 (2003)
8. J. Nishii, F.M. Hossain, S. Takagi, T. Aita, K. Saikusa, Y. Ohmaki, I. Ohkubo, S. Kishimoto, A. Ohtomo, T. Fukumura, F. Matsukura, Y. Ohno, H. Koinuma, H. Ohno, M. Kawasaki, Jpn. J. Appl. Phys. **42**, L347 (2003)
9. E.M.C. Fortunato, P.M.C. Barquinha, A.C.M.G.G. Pimentel, A.M.F. Goncalves, A.J.S. Marques, R.F.P. Martines, L.M.N. Pereira, Appl. Phys. Lett. **85**, 2541 (2004)
10. E. Fortunato, P. Barquinha, A. Pimentel, A. Goncalves, A. Marques, L. Pereira, R. Martins, Thin Solid Films **487**, 205 (2005)
11. Y. Ohya, T. Niwa, T. Ban, Y. Takahashi, Jpn. J. Appl. Phys. **40**, 297 (2001)
12. B.J. Norris, J. Anderson, J.F. Wager, D.A. Keszler, J. Phys. D: Appl. Phys. **36**, L105 (2003)
13. S.K. Volkman, B.A. Mattis, S.E. Molesa, J.B. Lee, A. de la Fuente Vornbrock, T. Bakhishev, V. Subramanian, in *Tech. Dig. IEEE Int. Electron Device Meet.* (2004), p. 769
14. P.M. Smith, P.G. Carey, T.W. Sigmon, Appl. Phys. Lett. **70**, 342 (1997)
15. N. Misra, L. Xu, Y. Pan, N. Cheung, C.P. Grigoropoulos, Appl. Phys. Lett. **90**, 11111 (2007)
16. P.L. Washington, H.C. Ong, J.Y. Dai, R.P.H. Chang, Appl. Phys. Lett. **72**, 3261 (1998)
17. I. Ozerov, M. Arab, V.I. Safarov, W. Marine, S. Giorgio, M. Sentis, L. Nanai, Appl. Surf. Sci. **226**, 242 (2004)
18. H. Pan, S.H. Ko, C.P. Grigoropoulos, Appl. Phys. A **90**, 247 (2008)
19. A. Plech, V. Kotaidis, S. Gresillon, C. Dahmen, G. Plessen, Phys. Rev. B **70**, 195423 (2004)
20. K. Vanheusden, W.L. Warren, C.H. Seager, D.R. Tallant, J.A. Voigt, B.E. Gnade, J. Appl. Phys. **79**, 7983 (1996)
21. I. Ozerov, D. Nelson, A.V. Bulgakov, W. Marine, M. Sentis, Appl. Surf. Sci. **212**, 349 (2003)
22. S.H. Ko, J. Chung, H. Pan, C.P. Grigoropoulos, D. Poulikakos, Sens. Actuators A: Phys. **134**, 161 (2007)
23. S.H. Ko, H. Pan, C.P. Grigoropoulos, C.K. Luscombe, J.M.J. Fréchet, D. Poulikakos, Appl. Phys. Lett. **90**, 141103 (2007)
24. S.H. Ko, H. Pan, C.P. Grigoropoulos, C.K. Luscombe, J.M.J. Fréchet, D. Poulikakos, Nanotechnology **18**, 345202 (2007)
25. S.H. Ko, I. Park, H. Pan, C.P. Grigoropoulos, A.P. Pisano, C.K. Luscombe, J.M.J. Fréchet, Nanoletters **7**(7), 1869 (2007)